Reactivity of Fluorinated Si(100) with F_2

D. P. Pullman

Department of Chemistry, San Diego State University, San Diego, California 92182

A. A. Tsekouras

Department of Chemistry, University of Athens, Athens, Greece GR-15771

Y. L. Li, J. J. Yang, M. R. Tate, D. B. Gosalvez, K. B. Laughlin, M. T. Schulberg, and S. T. Ceyer*

Department of Chemistry, Massachusetts Institute of Technology, Cambridge, Massachusetts 02139

Received: July 7, 2000

The dissociative chemisorption of F_2 on the Si(100)(2 × 1) surface saturated with 1 monolayer (ML) of fluorine is investigated as a function of the incident F_2 translational energy. At energies below 3.8 kcal/mol, no reaction with the Si−Si bonds occurs. Above this threshold, the probability of dissociative chemisorption rises linearly with the normal component of the incident translational energy up to a value of 3.6×10^{-3} at 13 kcal/mol. The relatively small effect of translational energy implies a late barrier in the potential energy surface for the interaction of F_2 with the Si−Si bonds. These probabilities are measured by exposing the fluorine-saturated surface to supersonic F_2 beams of variable energy, followed by thermal desorption measurements to determine the resulting fluorine coverage. Information regarding the specific Si−Si site (Si−Si dimer or Si−Si lattice bonds) at which the translationally activated reaction occurs is obtained from He diffraction measurements. The intensity of the diffracted beams is monitored after exposing the fluorine-saturated surface to F_2 of variable energy. The intensities remain constant after exposure to low-energy (<3.8 kcal/mol) F_2, whereas they decline monotonically as a function of F_2 normal energy above the 3.8 kcal/mol threshold. Moreover, the similarity of the relative cross sections for diffusive scattering measured after exposure to translationally fast F_2 to those measured after Ar^+ ion bombardment strongly suggests that the reaction does not occur preferentially at the Si−Si dimer bonds, which are the weakest Si−Si bonds in the system. Reaction at Si−Si lattice bonds also occurs, leading to surface disorder. Additional data show that for submonolayer coverages generated from low energy F_2, no reaction with Si−Si bonds occurs, while exposure to high-energy F_2 leads to reaction with Si−Si bonds.

I. Introduction

Recently, the mechanism for the dissociative chemisorption of F_2 on Si(100)2 × 1 was shown to proceed by atom abstraction.[1−3] As a F_2 molecule incident at low translational energies (<1.5 kcal/mol) approaches a Si surface at 250 K, a Si dangling bond abstracts one of the F atoms, which is then adsorbed at that site, while the complementary F atom is expelled. The complementary F atom can be expelled with a trajectory directed away from the surface, and thus, it becomes a gas-phase F atom. This reaction channel is called single-atom abstraction. Alternatively, it can be expelled with a trajectory aimed toward the surface where it may encounter a dangling bond and adsorb, resulting in a channel termed two-atom adsorption. Once the 1 monolayer (ML) of dangling bond sites is saturated with fluorine, the atom abstraction mechanism for dissociative chemisorption ceases. In fact, the probability for F_2 dissociative chemisorption approaches zero at 1 ML of fluorine coverage. The ordered, fluorine-saturated Si(100) surface becomes essentially passivated toward F_2 incident at thermal energies. Atom abstraction in this system is a facile, nonactivated mechanism for the saturation of dangling bond sites present on the clean Si(100) surface and requires no cleavage of the Si−Si σ bonds of the lattice.

Additional dissociative chemisorption of F_2 onto this fluorine-saturated surface in order to increase the fluorine coverage beyond 1 ML requires Si−Si bond cleavage. However, the passivity of the fluorinated surface signals that the F_2 incident at thermal translational energies cannot effect such Si−Si bond cleavage. This lack of reactivity can be understood as a consequence of the inability of the thermal energy of F_2 to overcome the activation barrier to reaction with the already-filled silicon bonding orbitals. Although cleavage of one Si−Si bond and one F−F bond to form a new Si−F bond,

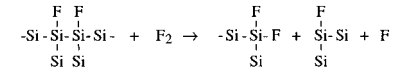

is exothermic by approximately 56 kcal/mol (using 148 kcal/mol for Si−F bond energy,[4] 54 kcal/mol for Si−Si bond energy,[5] and 38 kcal/mol for F_2 bond energy), a significant barrier between the reactant and product states may arise from the repulsive interaction between the filled valence Si orbitals and the closed-shell F_2 molecule. This repulsive interaction must

10.1021/jp002443v CCC: $20.00
Published on Web 12/15/2000

be overcome in order for the incoming F_2 to approach a Si lattice atom closely enough for a Si−F bonding interaction to form and, thus, for Si−Si bond cleavage to occur. It is a goal of this study to determine whether this potential energy barrier to Si−Si bond cleavage and subsequent F_2 dissociative chemisorption may be overcome by increased F_2 translational energy, thus providing a means to initiate the dissociative chemisorption of F_2 on the fluorine-saturated surface. It is also a goal of this study to determine whether the translationally activated reaction occurs preferably at the Si−Si dimer bonds. These bonds are the weaker Si−Si bonds because the Si atoms comprising the dimer are both bonded to a F atom. Alternatively, the reaction may occur nondiscriminatorily at both the Si−Si dimer bonds and the Si−Si bonds between the Si surface atoms and those Si atoms one layer below, called here the Si−Si lattice bonds.

The integrated thermal desorption rates of the SiF_x products formed after exposure to F_2 are the bases for the determination of the F_2 dissociative chemisorption probabilities on the fluorine-saturated Si(100) surface as a function of the incident F_2 energy. Helium atom diffraction measurements provide the information regarding the site, Si−Si dimer or Si−Si lattice bonds, at which the translationally activated reaction on the fluorine-saturated surface occurs. To correctly interpret these measurements on the fluorine-saturated surface, it is necessary to understand both the thermal desorption behavior and the He diffraction spectra at lower fluorine coverages as well as the He diffraction spectrum from the clean Si(100)2 × 1 surface. Therefore, both measurements are described in detail in section III.

II. Experimental Section

The apparatus has been described in detail elsewhere.[6] The apparatus consists of two differentially pumped, supersonic molecular beam sources coupled to an ultrahigh vacuum chamber (base pressure of 5×10^{-11} Torr) containing the Si crystal, cylindrical mirror electrostatic energy analyzer for Auger spectroscopy, an ion sputtering gun, a residual gas mass analyzer, and a triply differentially pumped, line-of-sight, rotatable quadrupole mass spectrometer.

A. Molecular Fluorine Beams. The molecular beams are skimmed and collimated through three stages of differential pumping. Expansion of 700 Torr of gas from a room temperature orifice of 0.002″ diameter typically yields a nearly monoenergetic F_2 beam ($\Delta E/E = 0.08$) as measured by time-of-flight spectroscopy. Beams of F_2 (97%, Air Products, subsequently purified through a HF trap, Matheson) with various energies are produced by seeding techniques. Mixtures of 1% F_2 in Ar (99.9995%, Spectra Gases), 1% F_2 and 49% He (99.9995%, Spectra Gases) in Ar, 1% F_2 and 9% Ar in He, 1% F_2 and 3% Ar in He, and 0.25% F_2 in He produce average F_2 translational energies of approximately 1.3, 2.6, 7, 10, and 13 kcal/mol, respectively, after expansion. In these experiments, knowledge of the relative fluxes of the F_2 beams with different energies is critical. The relative F_2 fluxes are determined by the relative integrated time-of-flight signals, weighted by the velocity. This determination was described in detail previously.[2]

A very low-energy He beam is produced by the expansion of a mixture of 50% He in Ar for the purpose of He diffraction measurements. Its average velocity is 766 ± 65 m/s (0.27 kcal/mol), with a translational temperature of 2 K and an average wavelength of 1.33 ± 0.11(fwhm) Å. The angle of incidence of the beam on the crystal is varied by rotating the crystal around its axis that is perpendicular to the scattering plane. The scattering plane is defined by the axes of the two molecular beams and the differentially pumped quadrupole mass spectrometer. The incident angle is measured with respect to the normal angle to the crystal. At normal incidence, the beam illuminates a rectangular area with dimensions 0.250″ × 0.177″ positioned at the center of the 0.495″ diameter Si(100) crystal.

B. Si(100) Crystal. The crystal is mounted between two Ta clamps that are attached to the manipulator. The crystal can be cooled to 125 K and heated resistively to ∼1100 K. Its temperature is measured via a W−5%Re/W−26%Re thermocouple attached with a ceramic glue to the back of the crystal. The surface temperature is held constant at 250 K during F_2 exposure.

The Si crystal is cut along the (100) plane. Both lightly n-type and p-type doped Si with resistivities of 8−12 Ω cm have been used. No differences in reactivity have been observed for the two types of doping. The Si crystal is cleaned by a wet etching procedure[7] prior to installation into the vacuum chamber. The crystal is sputtered with 2 keV Ar^+ and subsequently annealed at 1100 K for 30 min. This process is repeated until C and O contamination is below the 1% sensitivity limit of Auger electron spectroscopy. No metal contamination, such as W, Ta, Cu, or Ni, is observed. The crystal is typically mounted such that the scattering plane is along the (10) direction of the crystal surface. Helium diffraction confirms the (2 × 1) periodicity of the reconstructed Si(100) surface. The crystal is sputtered and annealed each day to ensure surface cleanliness and order. A brief anneal of the crystal to about 1100 K after each F_2 exposure removes all fluorine and results in the recovery of the (2 × 1) periodicity of the surface. The crystal is replaced when an etch spot becomes visible, typically after several months of experiments. No difference in reactivity is observed over the lifetime of the crystal.

C. Detection Scheme. Thermal desorption and scattering measurements are made with a triply differentially pumped, rotatable quadrupole mass spectrometer with electron bombardment ionization. The detector rotates about the center point of intersection of the beam and the crystal. The angular range is 35−180.3° with respect to the beam. The solid angle subtended by the detector is 5.8×10^{-4} sr. The angular resolution in the scattering plane is 3.52°. The rotation of the crystal and the detector allow for a wide range of incident and detection angles. A pseudorandom chopper wheel with 255 slots and spinning at 280 or 400 Hz at the entrance to the detector allows for measurements of the velocity distribution of both the incident beam as well as the scattered products using a cross correlation TOF technique. The neutral flight path is about 29 cm.

III. Interaction of Thermal Energy F_2 with Si

A. Thermal Desorption Measurements of ≤1 ML Fluorine Adsorbed on Si(100). Signals are detected mass spectrometrically at $m/e = 47(SiF^+)$, $66(SiF_2^+)$, $85(SiF_3^+)$, and $104(SiF_4^+)$ as the fluorinated layer of a coverage of 1 ML or less thermally desorbs upon heating. Because the relative desorption rates at $m/e = 47(SiF^+)$ and $66(SiF_2^+)$ as a function of temperature are identical to each other, as are those at $m/e = 85(SiF_3^+)$ and $104(SiF_4^+)$, the SiF^+ and SiF_3^+ signal are concluded to originate from fragmentation of the parent molecules, SiF_2 and SiF_4, respectively, upon electron impact ionization. A previous study[8] also concludes that SiF_2 and SiF_4 are the only desorption products as a result of the interaction of F_2 with Si(100). The SiF_4 product is detected as SiF_3^+ at $m/e = 85$ in the present experiments because the signal at this mass is larger due to extensive fragmentation of SiF_4 to SiF_3^+ upon impact with 70 eV electrons.

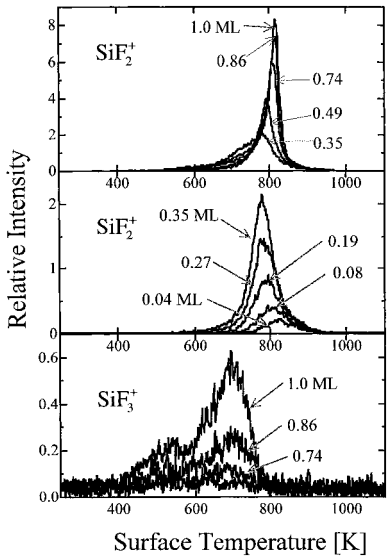

Figure 1. Thermal desorption spectra of SiF_2 and SiF_4 measured at $m/e = 66$ (SiF_2^+) and 85 (SiF_3^+) after sufficient F_2 exposure at $T_s = 250$ K to yield the fluorine coverages in ML F atom that are shown for each trace. Temperature ramp rate is 5 K/s. $E_i = 1.3$ kcal/mol.

Thermal desorption measurements of SiF_2 and SiF_4 are shown in Figure 1 for a variety of initial fluorine coverages measured in monolayers (ML), where 1 ML is equivalent to one F atom per Si surface atom. The coverages are calculated by scaling the signals integrated over temperature to the integrated signal at saturation coverage, which is known from an independent experiment to be equal to about 1 ML.[2] The F_2 is introduced to the Si surface at 250 K by exposure to a 1% F_2/Ar beam incident at 59°. The average F_2 translational energy, E_i, is 1.3 kcal/mol. The desorption products are detected by a triply differentially pumped mass spectrometer positioned along the normal angle to the surface. The SiF_2 thermal desorption rate is strongly dependent on the initial fluorine coverage. As the coverage increases to 0.35 ML (middle panel), the rate of SiF_2 desorption exhibits second-order kinetics, as indicated by the shift in the maximum desorption rate from 820 to 790 K. Above 0.35 ML (top panel), the maximum of the desorption rate shifts back up to 810 K as the coverage increases and the desorption rate becomes asymmetric, indicative of zero order behavior. The desorption of SiF_4 begins at coverages approaching 1 ML and exhibits first-order behavior, as shown in the bottom panel. Similar but not identical desorption kinetics has been observed in other laboratories.[9−11] The differences between them have been shown to arise from artifacts that arise from the use of a nondifferentially pumped detector.[2] Because the desorption kinetics are not critical to the goals of this experiment, a detailed analysis of them was not carried out.

However, knowledge of the relative amounts of the SiF_2 and SiF_4 desorption products is important for a valid interpretation of the effect of the F_2 translational energy. Unfortunately, the relative amount of each product is not simply a ratio of the two integrated signals for two reasons. First, because the desorbing SiF_2 and SiF_4 molecules are detected by a line-of-sight, differentially pumped, number density sensitive mass spectrometer whose acceptance angle is limited, the thermal desorption signals must be converted into flux measurements and must be normalized for differences in the angular distributions of the two desorbing products. Second, the thermal desorption signals of the two desorption products must be normalized for ionization efficiency in the electron bombardment ionizer of the detector and for transmission through the mass spectrometer. For example, the SiF_2 thermal desorption signal, $S_{SiF_2}(\theta,\varphi,T;\Theta)$, where θ is the desorption angle measured from the surface normal angle, φ is the azimuthal angle, T is the surface temperature, and Θ is the initial coverage, is related to its total thermal desorption yield $N_{SiF_2}(\Theta)$ by the following:

$$N_{SiF_2}(\Theta) = \int_{T_0}^{T_f}\int_0^{2\pi}\int_0^{\pi/2} C(\theta,\varphi)\frac{S_{SiF_2}(\theta,\varphi,T;\Theta)}{\sigma_{SiF_2} Id \eta_{SiF_2}} v_{SiF_2} \sin\theta \, d\theta \, d\varphi \, dT \quad (1)$$

In this expression, σ_{SiF_2} is the ionization cross section, Id is the product of the electron density with the length of the ionizing region, η_{SiF_2} is the transmission function, and v_{SiF_2} is the velocity. The geometric sensitivity factor, $C(\theta,\varphi)$, is determined by the surface-detector configuration.[12,13] Assuming that the angular and velocity distributions are each independent of the surface temperature and initial surface coverage, we can write eq 1 as

$$N_{SiF_2}(\Theta) = \frac{v_{SiF_2}}{\sigma_{SiF_2} Id \eta_{SiF_2}} \int_0^{2\pi}\int_0^{\pi/2} C(\theta,\varphi) D_{SiF_2}(\theta,\varphi) \sin\theta \, d\theta \, d\varphi \int_{T_0}^{T_f} S_{SiF_2}(T;\Theta) \, dT \quad (2)$$

where $D_{SiF_2}(\theta,\varphi)$ now represents the angular distribution of the desorbing SiF_2 and $S_{SiF_2}(T;\Theta)$ represents the thermal desorption signal measured at one angle. Therefore, the ratio of the total SiF_4 thermal desorption yield to that for SiF_2 can be written as

$$\frac{N_{SiF_4}(\Theta)}{N_{SiF_2}(\Theta)} = \frac{v_{SiF_4}}{v_{SiF_2}} \frac{\sigma_{SiF_2}}{\sigma_{SiF_4}} \frac{\eta_{SiF_2}}{\eta_{SiF_4}} \frac{\int_0^{2\pi}\int_0^{\pi/2} D_{SiF_4}(\theta,\varphi) \sin\theta \, d\theta \, d\varphi}{\int_0^{2\pi}\int_0^{\pi/2} D_{SiF_2}(\theta,\varphi) \sin\theta \, d\theta \, d\varphi} \frac{\int_{T_0}^{T_f} S_{SiF_4}(T;\Theta) \, dT}{\int_{T_0}^{T_f} S_{SiF_2}(T;\Theta) \, dT} \quad (3)$$

The literature value for the ionization cross section,[14] σ_{SiF_2}, of $SiF_2 \rightarrow SiF_2^+ + e^-$ is 1.38 Å^2, while that[15] for $SiF_4 \rightarrow SiF_3^+ + F + e^-$ is 12 Å^2. The ratio of the SiF_2 and SiF_4 transmission functions measured at $m/e = 66$ and 85, respectively, is one. The procedure for measuring the transmission functions is detailed elsewhere.[12,13,16,17] Because of the tedious nature of measuring time-of-flight distributions during a thermal desorption measurement and because highly accurate knowledge of the ratio of the product yields is not necessary for a valid interpretation of the experiment in section IV, the time-of-flight spectra of SiF_2 and SiF_4 are measured under steady-state conditions at surface temperatures of 1000 and 675 K, respectively, as a beam of F_2 with 11.3 kcal/mol of energy is incident on the surface at 45° and 35°, respectively. The detector is positioned along the normal angle. The SiF_2 distribution is well fit by a Maxwell−Boltzmann distribution at approximately the surface temperature, 950 K. Given this observation, the SiF_2 in the thermal desorption experiment is assumed to desorb in thermal equilibrium with the surface at 800 K, which is the temperature of the maximum desorption rate. Thus, the average velocity for a flux distribution of SiF_2 desorbing at 800 K is 597 m/s. Unlike SiF_2, the time-of-flight distribution of SiF_4 cannot be fit by a Maxwell−Boltzmann distribution at the surface temperature of 675 K. Rather, the distribution is fit with a flow temperature of 2450 K and a beam temperature of 740 K, indicating that SiF_4 is scattered from the surface with an energy substantially above that corresponding to thermal equi-

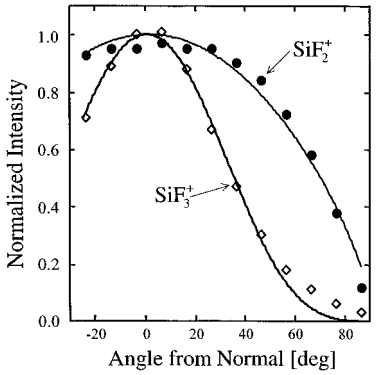

Figure 2. Temperature-integrated SiF_2^+ and SiF_3^+ thermal desorption signals resulting from desorption of $\Theta = 1$ ML of fluorine as a function of the scattering angle, θ, as measured from the surface normal. Measurements are normalized at the normal angle. Solid lines represent fits of the functional form $\cos^x(\theta)$, where $x = 0.7$ and 3.5 for SiF_2^+ and SiF_3^+, respectively.

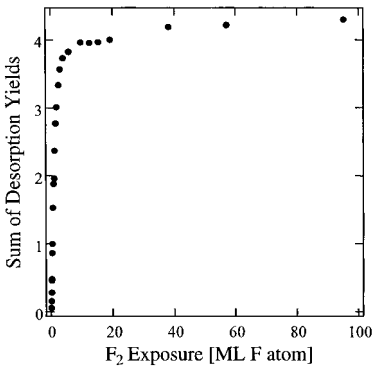

Figure 3. Sum of the total SiF_2 and SiF_4 thermal desorption yields (see text) vs F_2 exposure.

librium. Since the steady-state time-of-flight measurement is carried out just 25 K below the temperature at which the desorption rate of SiF_4 is a maximum, the average velocity of a flux distribution of thermally desorbed SiF_4 is assumed to be equivalent to that measured in the steady-state measurement, 862 m/s.

The penultimate factor in eq 3 is the ratio of the normalized thermal desorption signals integrated over scattering angles. Figure 2 shows the temperature-integrated SiF_2^+ and SiF_3^+ thermal desorption signals resulting from desorption of 1 ML of fluorine as a function of the scattering angle. They are normalized at 0° from the normal angle. The solid lines represent fits to $\cos^x(\theta)$, where $x = 0.7$ and 3.5 for SiF_2^+ and SiF_3^+, respectively. Both angular distributions are peaked at the normal angle, but that for SiF_2^+ is slightly broader than a cosine function, while that for SiF_3^+ is much narrower than a cosine function. Each distribution is then integrated over both scattering angles θ and φ, using the assumption that each distribution is azimuthally symmetric. The ratio of the integrated angular distributions is thus calculated to be 0.373.

The ratio of the total desorption yields, $N_{SiF_4}(\Theta)/N_{SiF_2}(\Theta)$, can now be calculated as a function of the initial coverage from the ratio of the thermal desorption signals integrated over temperature, $(\int S_{SiF_4}(T;\Theta)\,dT)/(\int S_{SiF_2}(T;\Theta)\,dT)$, using eq 3. As seen in Figure 1, the SiF_4 product is measurable only as the coverage nears 1 ML. While the ratio of the total desorption yields of SiF_4 to SiF_2 increases as the coverage increases from 0.86 to 1 ML, the relative yield of SiF_4 never exceeds 1.7% of the SiF_2 yield, even at F_2 exposures as large as 100 ML. The SiF_4 product is thought to be formed at defect sites. Indeed, scanning tunneling microscope images of Si(100) have revealed defect densities on the order of a few percent.[18] Thus, SiF_2 is the major product of the thermal decomposition of a Si(100) surface fluorinated with 1 ML or less. This fact will be important to the analysis in section IV of the effect of translational energy on the dissociation probability of F_2 on a fluorinated Si surface.

The aspect of these thermal desorption experiments motivating the present investigation is their demonstration that the dissociation probability of F_2 approaches zero as the fluorine coverage increases to 1 ML and slightly beyond. This fact can be seen in Figure 3, which shows a plot of a quantity proportional to the sum of the total SiF_4 and SiF_2 thermal desorption yields versus F_2 exposure, where the exposure is given in ML F atoms. The ordinate is given by

$$\frac{N_{SiF_2}(\Theta) + N_{SiF_4}(\Theta)}{(\upsilon_{SiF_2}/\sigma_{SiF_2} I d \eta_{SiF_2}) \int\int C(\theta,\varphi) D_{SiF_2}(\theta,\varphi) \sin\theta\, d\theta\, d\varphi} = \int_{T_0}^{T_f} S_{SiF_2}(T;\Theta)\, dT + 2\frac{\upsilon_{SiF_4}}{\upsilon_{SiF_2}}\frac{\sigma_{SiF_2}}{\sigma_{SiF_4}}\frac{\eta_{SiF_2}}{\eta_{SiF_4}}\frac{\int\int D_{SiF_4}(\theta,\varphi)\sin\theta\, d\theta\, d\varphi}{\int\int D_{SiF_2}(\theta,\varphi)\sin\theta\, d\theta\, d\varphi} \int_{T_0}^{T_f} S_{SiF_4}(T;\Theta)\, dT \quad (4)$$

Note that the sum of the total SiF_4 and SiF_2 thermal desorption yields is also proportional to the fluorine coverage. In Figure 3, this sum is expressed in arbitrary units, so it is useful only for comparison of the yield or coverage at different exposures. Figure 3 shows the total fluorine coverage to increase rapidly upon initial exposure to the F_2 beam and then to become almost constant at high exposures. A previous analysis[2] has shown that this constant coverage is achieved when the exposure is sufficiently high for the coverage to reach the saturation value of 1 ML. However, careful inspection of Figure 3 reveals that the sum of the total desorption yields, and hence the coverage, is not exactly constant at very high F_2 exposures and that therefore the probability of F_2 dissociative chemisorption is not exactly zero. Recall that the slope of this plot at any exposure is directly proportional to the F_2 dissociative chemisorption probability. An upper limit to the dissociation probability at 1 ML coverage can be determined by comparing the slope of the plot of the integrated yield versus F_2 exposure beyond 20 ML to the slope in the limit of zero exposure or coverage, where the dissociative chemisorption probability is known to be about one.[1,2] Analysis and calibration of the slope of the plot of the integrated yield versus F_2 exposure beyond 20 ML yields a value of $9(\pm1) \times 10^{-4}$ for the dissociative chemisorption probability of F_2 on a Si(100) surface covered with 1 ML of fluorine. These results clearly show that the F_2 dissociation probability, which is initially close to one on the unfluorinated surface, decays toward zero as the surface becomes passivated with a fluorine layer. It is the goal of this experiment to demonstrate that higher translational energies of F_2 will activate its dissociation on this fluorine-saturated Si(100) surface.

B. Surface Structure Determination by He Atom Diffraction. *1. Si(100).* A comparison of the He atom diffraction spectrum of an unfluorinated Si(100) surface to that of the fluorinated surface provides a basis for the interpretation of the structure of the fluorine overlayers. Since the primary goal of the diffraction studies is to monitor changes in the diffraction intensities as a result of exposures to varying energies of the incident F_2 beam, conditions must be found that maximize the

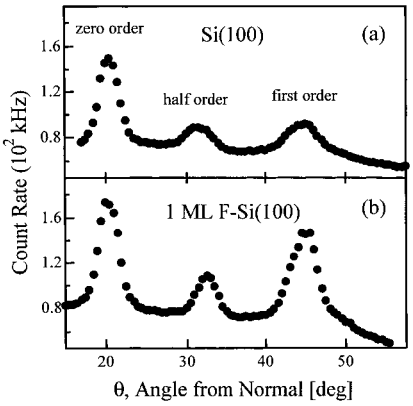

Figure 4. Helium signal scattered from Si(100) at 250 K as a function of the scattering angle, θ, with $\theta_i = 20°$: (a) clean surface and (b) $\Theta = 1$ ML of fluorine.

diffraction features. Comparison of spectra measured over a wide range of incident angles showed that a 20° or 33° incident angle maximized the zero, half-order, and first-order diffraction features for an incident He atom wavelength of 1.33 Å. The diffraction spectra shown here were measured over a range of surface temperatures, 250−300 K. Because this temperature range is below the surface Debye temperature of Si, spectra measured over this range are indistinguishable from each other. Lowering the temperature below 250 K has a minimal effect on the diffraction intensities.

Since the specular intensity is very sensitive to the presence of adsorbed contaminants, it was monitored often during the course of an experiment. If necessary, the crystal was heated to 1100 K and maintained there for 10 s. This procedure was sufficient to recover diffraction intensities, even after exposure to F_2 at high incident energies, to within 10% of those obtained immediately following the sputtering/annealing cycle.

A typical diffraction spectrum over a narrow range of scattering angles, obtained by scattering a beam of He atoms with an average wavelength of 1.33 ± 0.11(fwhm) Å and an incident angle, θ_i, of 20°, is shown in Figure 4a. The angular width of the beam in the scattering plane is 2°. The He beam is modulated at 150 Hz with a tuning fork chopper for the purpose of background subtraction. The scattered He signal is detected by the triply differentially pumped mass spectrometer as a function of the scattering angle in the scattering plane. The detector is rotated in steps of 0.5° from 15−55° with respect to the surface normal in the forward scattering direction.

Evident in the spectrum of Figure 4a are the zero, half-order, and first-order diffraction features. A lattice spacing of 3.73 Å, which is within 3% of the known value, is determined from the peak positions. Also immediately noticeable is the broad width of the diffraction features. The full width at half-maximum of the specular, half-order, and first-order features are 2.9°, 3.7°, and 4.4°, respectively. The breadth of these features is a consequence of the limited transfer width of the scattering apparatus and in particular, a consequence of the large acceptance angle of the detector. The sizes of the entrance slits on the detector were chosen to optimize the intensity of the reactively scattered signal rather than the spatial resolution of elastically scattered signal. The widths of these features can be reproduced well in a simulation that convolutes the finite size of the incident beam and detector chamber entrance slits with the distribution of velocities of the incident beam.[12]

The diffraction spectrum is typical of a Si(100) surface that has undergone the well-known (2 × 1) reconstruction.[19] In real space, each Si surface atom is a member of a Si dimer pair and has one dangling bond. The Si dimer pairs form rows where the distance between each dimer pair in the same row is the same as the lattice spacing of the bulk Si, while the distance between Si dimer pairs in adjacent rows is twice the bulk Si lattice spacing, thereby forming a (2 × 1) surface unit cell. It is the periodic doubling of the lattice spacing in the direction perpendicular to the rows of the dimers that gives rise to the half-order diffraction feature. The half-order diffraction feature is therefore a signature for the presence of the Si dimers. It will be used in this study as an indicator for the cleavage of Si−Si bonds upon the adsorption of fluorine.

The half-order diffraction feature is most intense when the beam is parallel to the dimer rows. This azimuthal orientation is the case in the spectrum in Figure 4a. It should be noted that there are two domains of the (2 × 1) surface unit cells where the dimer rows of one domain are perpendicular to those of the other. Therefore, the half-order diffraction peak is evident when the azimuthal orientation of the beam is along the [10] or the [01] direction.

2. Fluorinated Si(100). The purpose for studying the reaction of F_2 with Si using He diffraction is to determine the structure of the fluorinated surface. In principle, both the fluorine adsorption site and the location of the Si atoms as well as the extent of Si−Si bond cleavage are identifiable from the diffraction spectra. However, without an extensive high-resolution data set over a wide range of incident energies and angles coupled with simulations, the F adsorption site is not unequivocally determinable. Nevertheless, changes in the diffraction spectrum measured upon exposure to F_2 do reveal which periodic structures of the unfluorinated surface have been disrupted and which ones have been maintained. In this way, the identity of the Si surface atoms directly involved in the reaction is determined.

Figure 4b shows a diffraction spectrum measured under the same conditions as those in Figure 4a but measured from a Si surface covered with 1 ML of fluorine. Comparison of these spectra reveals that the spectrum from the fluorinated surface is very similar to that from the clean surface, indicating that the fluorine overlayer formed at saturation coverage has the same (2 × 1) periodicity or unit cell as that of the underlying Si substrate. This observation, coupled with the knowledge that the saturation coverage is about 1 ML, suggests strongly that each dangling bond is decorated by one fluorine atom. Because the dangling bond sites are not already involved in a bonding interaction, adsorption on them requires no Si−Si bond cleavage, leaving the Si−Si dimer bond, which gives rise to the half-order diffraction feature, still intact.

The inertness of the (2 × 1) structure of the fluorine overlayer to further exposures of thermal energy fluorine can be clearly seen in measurements of the intensities of the zero, half-order, and first-order diffraction features as a function of F_2 exposure as shown in Figure 5 by the solid lines. These measurements are made by directing a beam containing 1%F_2/49%He/50%Ar at the crystal. As the fluorine reacts with the Si, the He carried in the same beam is monitored for coherent scattering as an indicator of change in the surface periodicity. Each trace represents a separate exposure to the beam while the He signal is measured with the detector positioned at the scattering angles corresponding to the zero, half-order, or first-order diffraction features. The F_2 and the He are incident at 33° from the normal angle. The average energy of the incident F_2 is 2.5 kcal/mol, and the average wavelength of the He is 1.33 ± 0.11(fwhm) Å. The intensity of each beam is normalized to its value at zero exposure. At low exposures, just as the fluorine begins to adsorb,

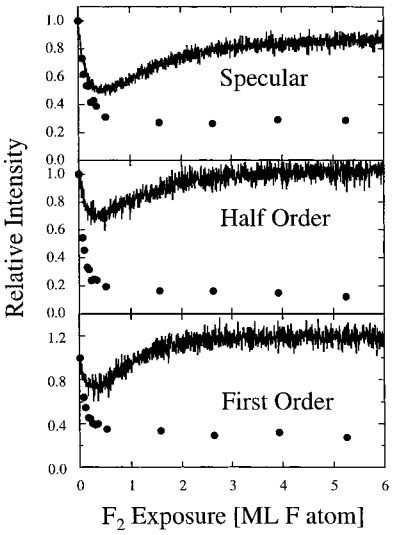

Figure 5. Intensities of the specular, half-order, and first-order He diffraction beams as a function of exposure to F_2 incident at 2.5 kcal/mol (solid line) and at 13 kcal/mol (circles). The intensity of each beam is normalized to its value at zero exposure. High-energy data discussed in section IV.C.

the intensity of the diffraction features drops, indicating that the order of the surface has been disrupted. With higher exposures, the intensity recovers and becomes constant and remains so even at very long exposures.

The loss of intensity of the diffraction features upon the initial exposure to F_2 can be understood in terms of the partial fluorine coverage. At zero exposure, the surface is a well-ordered array of dimer rows with a (2×1) unit cell. As F_2 reacts with the surface, the F atoms attach to the dangling bonds in a random manner. The presence of a F atom changes the interaction potential of the He atom with this surface unit cell, thereby making it different from the surrounding unit cells that do not yet include a F atom. Although no Si−Si bonds have been broken, the original periodicity of the clean (2×1)Si surface has been disrupted, which results in the loss of coherency of the scattered He beam. However, as the coverage of fluorine increases, a transition to a new order is observed as an increase in the diffraction intensities when the periodicity of the fluorinated surface unit cells begins to predominate over the unfluorinated ones. Eventually, as all of the dangling bonds are fluorinated and each unit cell becomes identical to each of its neighbors, the original (2×1) periodicity is recovered even though the interaction potential of the He atom with the surface has changed. As observed in Figure 5, the diffraction intensities are again at maximal values but have absolute values different from those of the clean surface because the interaction potential has changed.

Once formed, this newly ordered fluorinated surface is resistant to further attack by F_2. The invariance of the diffraction intensities and the surface periodicity at high F_2 exposures indicates that the surface is saturated with fluorine and that it is no longer reactive with F_2. These observations are consistent with a near-zero dissociative chemisorption probability of 9×10^{-4} determined from the thermal desorption measurements in the previous section. The termination of atom abstraction at the saturation coverage is also consistent with the assignment of the fixed number of dangling bond sites as the adsorption sites for F on Si(100).[1,2] The dissociative chemisorption of F_2 ceases because all of the dangling bonds are filled. The F_2 incident at thermal energies is unable to break Si−Si bonds.

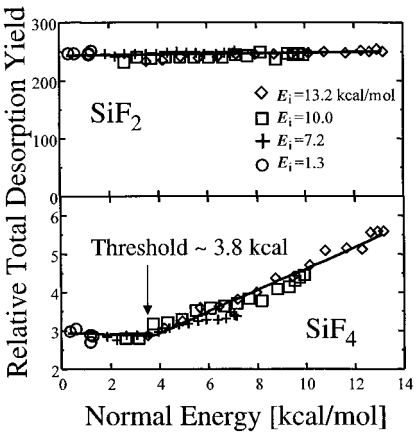

Figure 6. Total SiF_2 and SiF_4 thermal desorption yields, $N_{SiF_2}(\Theta)$ and $N_{SiF_4}(\Theta)$, measured at four total energies, E_i, and at 5−8 incident angles are plotted, in arbitrary units, as a function of the normal component of the incident F_2 energy. Solid lines are the linear least-squares fits to the data. For SiF_4, fits are constrained to intersect at 3.8 kcal/mol.

IV. Results

A. F_2 Dissociation Probability on F/Si(100) as a Function of F_2 Energy. The experiments in this section probe whether the dissociative chemisorption of F_2 on a fluorine-saturated Si(100) surface can be translationally activated. The measurements of the effect of the translational energy of the incident F_2 on its probability of dissociative chemisorption are carried out on a Si(100) surface that is covered with 1 ML of fluorine, as opposed to the clean surface. Measurements of the effect of F_2 translational energy on the fluorine-saturated surface probes solely the activation barrier to F_2 dissociative chemisorption when disruption of the Si−Si bonds are involved. In contrast, such energy dependence measurements on the clean surface are convoluted by the effect of translational energy on the atom abstraction mechanism.[11,20] The use of a fluorine-saturated surface precludes the nonactivated atom abstraction reaction, thus isolating the effects of enhanced F_2 translational energy in overcoming the barrier to Si−Si bond cleavage.

A fluorine-saturated surface is prepared by exposing the clean Si(100) surface held at 250 K to sufficient F_2 to reach a constant fluorine coverage, known to be 1 ML, as shown in Figure 3. The F_2 is incident with 1.3 kcal/mol of energy and with angles varying between 0° and 60°. The fluorine-saturated surface is then exposed to 19 ML of F_2 incident at 1.3, 7.2, 10, or 13 kcal/mol and incident with angles varying between 0° and 60°. The incident angle at which the exposure to higher-energy F_2 is carried out is the same as that used to prepare the fluorine-saturated surface. This procedure ensures that the surface area that is exposed to the high-energy F_2 is equivalent to the area that is covered with 1 ML of fluorine. Note that the time of exposure to the F_2 beam is adjusted for the relative fluxes of each of the beams at different energies and for the different incident angles so that the exposure, 19 ML, is the same for each beam. No etching, as evidenced by the absence of SiF_4 desorption, is observed under these conditions of low F_2 flux. The surface temperature is then increased at a rate of 5 K/s to 1110 K while the signal at $m/e = 66$, corresponding to SiF_2^+ from SiF_2, and at $m/e = 85$, corresponding to SiF_3^+ from SiF_4, is monitored along the surface normal by the line-of-sight, differentially pumped mass spectrometer.

The total SiF_2 and SiF_4 thermal desorption yields, $N_{SiF_2}(\Theta)$ and $N_{SiF_4}(\Theta)$, measured at four total energies and at 5−8 incident angles are plotted, in arbitrary units, as a function of the normal component of the incident energy in Figure 6. The normal

incident energy is defined as the energy associated with the component of incident momentum oriented normal to the macroscopic surface, and is calculated as $E_i \cos^2\theta_i$, where E_i is the incident energy and θ_i is the incident angle. It is apparent from the plots that the SiF_2 yield does not depend on the normal energy of the incident F_2, while the SiF_4 yield exhibits a linear dependence on it above a threshold value estimated from the plot to be about 3.8 kcal/mol. For a fixed 19 ML exposure of F_2 to a fluorine-saturated surface, the SiF_4 yield is observed to be larger by approximately a factor of 2 for a F_2 exposure at 13 kcal/mol as compared to thermal energies. There is no effect of energy on the F_2 dissociative chemisorption probability between 0.4 and 3.8 kcal/mol. Recall that the probability of F_2 dissociative chemisorption at thermal energies, which corresponds to energies below 3.8 kcal/mol in Figure 6, was estimated above as 9×10^{-4}. Thus, the probability of dissociative chemisorption of F_2 on a fluorinated surface increases from 9×10^{-4} to 3.6×10^{-3} as the normal component of the translational energy increases from 3.8 kcal/mol to 13 kcal/mol. The value of 3.6×10^{-3} is obtained by taking the factor of 2 increase observed in the SiF_4 yield in Figure 6 and multiplying it by the number of F_2 molecules contained in SiF_4. The factor of 4 increase in the dissociation probability corresponds to only a small increase in the total fluorine coverage. Note that the SiF_4 product yield from desorption of 1 ML of fluorine that has been deposited with energies below 3.8 kcal/mol is about 1.2% of the total fluorine coverage. Thus, the factor of 2 increase in the SiF_4 product yield represents a 4.8% increase in the fluorine coverage. Therefore, the dissociation probability of 3.6×10^{-3} at 13 kcal/mol is considered an "initial" dissociation probability on the fluorinated-Si(100) surface.

It is important to note that the independence of the SiF_2 yield and the dependence of the SiF_4 yield on the F_2 energy do not reflect a direct mechanism for SiF_4 formation involving the impact of a F_2 molecule on an adsorbed SiF_2 species. Rather, the independence of the SiF_2 yield reflects the kinetics of the thermal desorption of the adsorbed fluorine. No matter how high the initial fluorine coverage is beyond 1 ML, the amount of SiF_2 that desorbs is the same, because the SiF_2 arises from the desorption of the final monolayer of fluorine. Therefore, as the fluorine coverage grows beyond 1 ML, as in this case of the translational activation of F_2, the SiF_2 yield remains constant while the SiF_4 yield grows in proportion to the fluorine coverage beyond 1 ML.

The observed dependence of the F_2 dissociation probability on the normal component of the incident energy implies that the barrier to dissociation is one-dimensional and oriented normal to the macroscopic surface plane. The threshold energy of 3.8 kcal/mol also implies that the lowest energy barrier on the fluorinated Si surface is approximately 3.8 kcal/mol. As discussed in the Introduction, the addition of fluorine beyond 1 ML necessitates that Si−Si bonds be broken. In the next section, He diffraction experiments are carried out in an attempt to determine whether the weakest Si−Si bonds, the Si−Si dimer bonds, are broken in preference to the Si−Si lattice bonds, the bonds between the top layer of Si atoms and the Si atoms in the second layer.

B. He Diffraction from Fluorinated Si(100) as a Function of F_2 Energy. A Si(100) surface covered with 1 ML of fluorine is prepared as described above. The use of a fluorinated surface precludes atom abstraction, thus isolating the effects of enhanced F_2 translational energy in overcoming the activation barrier to reaction at Si−Si bonds. This fluorinated surface at 250 K is then exposed to 19 ML of F_2 incident at various energies and angles, again as described above, and a helium diffraction spectrum is measured after each exposure. The resulting intensities of the specular, half-order, and first-order diffraction features are plotted as a function of the normal component of the incident F_2 translational energy in Figure 7. The diffraction intensities are observed to remain approximately constant from 0.4 to about 3.8 kcal/mol but then to decrease approximately linearly with increasing normal energy of the F_2 above 3.8 kcal/mol. It is evident that incident normal energies above 3.8 kcal/mol are effective both in disrupting the lattice structure of the fluorinated Si(100) surface and in increasing the fluorine coverage beyond 1 ML. Therefore, increases in fluorine coverage beyond 1 ML are associated with disorder.

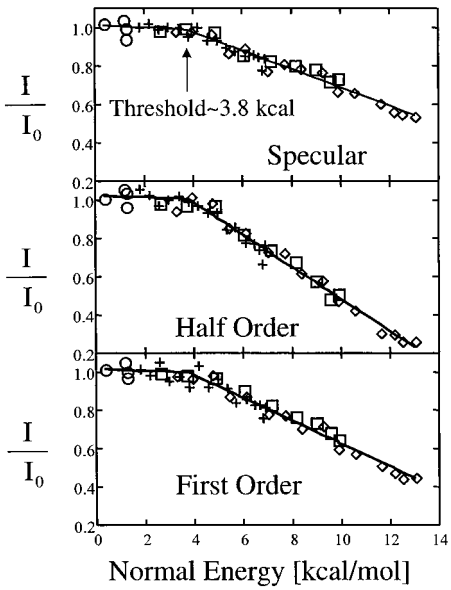

Figure 7. Intensities of the specular, half-order, and first-order diffraction beams plotted as a function of the normal component of the incident F_2 translational energy. The intensity of each beam is normalized to its value, I_o, from a Si surface saturated with 1 ML of fluorine. Solid lines are the linear least-squares fits to the data where fits are constrained to intersect at 3.8 kcal/mol. The symbols same as those in Figure 6.

The loss of diffraction intensity can be described quantitatively in terms of an increase in the concentration of "diffuse scattering sites" on the surface. A "diffuse scattering site" is defined as a site at which the surface periodicity has been disrupted in such a way so that its contribution to the coherent scattering of incident helium is negligible. Helium atoms incident at this site will scatter diffusely, and will thus not contribute to the coherently scattered or diffracted intensity. A detailed framework for analysis of the losses in diffraction intensities due to defects, which function as diffuse scattering sites, has been presented by Comsa[21] and is applied to the present problem. Coherent scattering intensities are assumed to derive only from those parts of the surface maintaining the original structure of the (2×1) reconstruction, i.e., defect-free regions of the surface. More precisely, for a particular surface unit cell to contribute to the coherently scattered intensity, an area F_D, centered at the unit cell, must be defect-free, where F_D is referred to as the quantum mechanical cross section for diffuse scattering. Therefore, $F_D n_s$ neighboring sites must be free of defects, where n_s is the density of surface sites in atoms/cm^2. If the defects are randomly distributed on the surface, the probability of having $F_D n_s$ defect-free neighboring sites is $(1 - \Theta_D)^{F_D n_s}$, where Θ_D is the fraction of surface sites possessing defects and $(1 - \Theta_D)$ is therefore the fraction of defect-free sites. Assuming that the defect sites act as perfectly diffuse

scatterers, and thus do not contribute to any coherent scattering amplitude, the quantum mechanical coherently scattered amplitude A_s (relative to the amplitude A_o from the defect-free surface) may be given as

$$\frac{A_s}{A_0} = (1 - \Theta_D)^{F_D n_s} \tag{5}$$

and thus the coherently scattered intensity given as

$$\frac{I}{I_0} = \left(\frac{A_s}{A_0}\right)^2 = (1 - \Theta_D)^{2F_D n_s} = (1 - \Theta_D)^{\Sigma n_s} \tag{6}$$

where $\Sigma = 2F_D$. Furthermore, in the limit of $\Theta_D \ll 1$, $(1 - \Theta_D)^{\Sigma n_s}$ may be expressed in terms of the binomial expansion to yield

$$(1 - \Theta_D)^{\Sigma n_s} \approx 1 - \Theta_D \Sigma n_s \tag{7}$$

It then follows that

$$I/I_o \approx 1 - \Theta_D \Sigma n_s \tag{8}$$

where Σ is the cross section for diffuse scattering which is a constant for a given diffraction feature and type of diffuse scattering site. The relative loss in diffraction intensities is thus a linear function of the concentration of defect sites on the surface.

Figure 7 displays the diffraction intensities, I/I_o, as a function of the normal energy of the incident F_2. Note that it has the same functional form as eq 8. Since the F_2 exposure has been adjusted experimentally to yield an equivalent F_2 exposure of 19 ML at each beam energy, the intensity losses can be considered linearly proportional to the fraction of defect sites, Θ_D, created at each normal energy. Therefore, the slopes of each plot are proportional to Σn_s, labeled below as *slope*, as long as the coverage of defect sites is sufficiently low such that there is negligible overlap between them. Thus, the data given in Figure 7 demonstrate that the probability of creating a defect site on the fluorinated surface varies linearly with F_2 normal incident energy above a threshold of ~3.8 kcal/mol. Since independent measurements for Σ and Θ_D are not available, neither Σ nor Θ_D can be determined absolutely.

The creation of surface defects effected by F_2 at higher incident translational energies corresponds to disruption of the Si−Si bonds. An interesting question arises, however, in determining whether F_2 reacts selectively with certain bonds on the fluorinated Si(100) surface. Most notably, examination of the plot of diffraction intensities vs F_2 normal incident energy given in Figure 7 reveals that the half-order diffraction feature loses intensity fastest as a function of the F_2 normal energy. After a F_2 exposure at 13 kcal/mol normal incident energy, the half-order feature is reduced to less than 30% of its original intensity, whereas both the specular and first-order intensities retain well over 40% of their original intensities. The question thus arises as to whether the enhanced rate of decline in the half-order diffraction intensity is due to selective reaction at the Si−Si dimer bonds which give rise to the half-order feature, or whether the effect is due solely to a larger cross section, Σ, for diffuse scattering from random defects for the half-order feature. Note that selective cleavage of the Si−Si dimer bonds would eliminate the periodicity doubling from which the half-order feature derives, instead reverting the surface to a (1×1) periodicity, from which strong specular and first-order features would be expected. It is thus plausible that the half-order intensity drops faster than the specular or first-order feature due to selective Si−Si bond cleavage at the surface dimers.

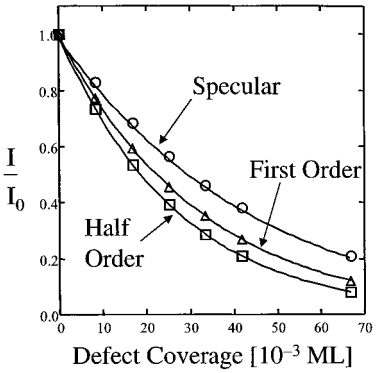

Figure 8. Intensities of the specular, half-order, and first-order diffraction beams plotted as a function of the coverage of defects induced by the impact of Ar^+ ions. The intensity of each beam is normalized to its value, I_o, from a Si surface saturated with 1 ML of fluorine. Solid lines are fits to eq 6.

This question may be addressed by generating random defect sites on the surface, and determining directly the cross sections for diffuse scattering for the specular, half-order, and first-order diffraction features. Random surface defects are created by bombarding the surface with 2 kV Ar^+ ions. These high-energy Ar^+ ions are expected to cause nonselective bond rupture upon impact because their incident energy is many times larger than the Si−Si bond energies. Their collision with the lattice results in a range of displaced Si atoms of at least 15.5 Å radius from the point of impact.[22] Each incident Ar^+ ion is assumed to create such a random defect at the surface with unit probability. The coverage of surface defects is thus varied by changing the length of exposure to a given current of Ar^+ ions.

One monolayer of fluorine adsorbed on Si(100) is prepared as in the diffraction experiments described above. The Ar^+ bombardment is performed with an ion sputtering gun whose emission is set to 3 mA and whose applied beam voltage is 2 kV. The Ar partial pressure in the chamber is increased to 5×10^{-6} Torr, providing an Ar^+ ion current to the crystal of 175 nA. This current is assumed to be evenly distributed over the crystal face, as well as the front crystal clamps, in the calculations of the Ar^+ ion flux. The He probe beam is identical to that employed for the normal energy scaling experiments just described.

Helium diffraction intensities are displayed as a function of the coverage of Ar^+-induced surface defects in Figure 8. The abscissa of this plot is determined by assuming that each incident Ar^+ ion generates the formation of one surface defect. The decay in the intensity of each diffraction feature is fit to the functional form given in eq 5, where the surface defect coverage, expressed in terms of ML, is taken directly as Θ_D. These fits yield the following values for the cross sections for diffuse scattering for each diffraction feature:

$$\Sigma_0 = 330 \text{ Å}^2$$

$$\Sigma_{1/2} = 540 \text{ Å}^2$$

$$\Sigma_1 = 460 \text{ Å}^2$$

where Σ_0, $\Sigma_{1/2}$, and Σ_1 are the standard cross sections for diffuse scattering for specular, half-order, and first-order diffraction, respectively. As described above, the corresponding cross sections, Σ_0, $\Sigma_{1/2}$, and Σ_1, cannot be determined for F_2-induced surface defects, since the surface defect coverage, Θ_D, is not

accurately known in those experiments. However, the relative slopes, *slope*, for the decay in diffraction intensities given in Figure 7 may be compared to the relative cross sections obtained from Figure 8, since these slopes are proportional to cross sections for diffuse scattering for each of the diffraction features. A comparison of the relative cross sections obtained from F_2- and Ar^+-induced surface defects yields the following:

$$slope_0:slope_{1/2}:slope_1 = 1:1.8:1.3$$

$$\Sigma_0:\Sigma_{1/2}:\Sigma_1 = 1:1.6:1.4$$

Although the values for the cross section ratios display only moderate agreement, note that in both cases the half-order cross section is larger than the first order cross section, which in turn is larger than the specular cross section for diffuse scattering. It may thus be concluded that the faster rate of decline of the half-order diffraction intensity observed in Figure 7 does not necessarily imply selective breaking of the surface dimer bonds, but rather is indicative of a larger diffuse scattering cross section for the half-order diffraction feature.

A description of the reaction of F_2 on the fluorinated Si(100) surface emerges as follows: At enhanced translational energies, F_2 reacts with the Si−Si dimer and lattice bonds of the fluorinated surface, disordering the surface structure and destroying the periodicity. The probability of reaction or dissociative chemisorption scales linearly with normal incident energy above a threshold of approximately 3.8 kcal/mol, as evidenced by both the increase in the coverage and the decrease in the surface order. The Si−Si dimer bonds are not preferentially cleaved by incident F_2.

C. He Diffraction from Si(100) as a Function of F_2 Energy. The above results demonstrate the disruption of Si−Si dimer and lattice bonds on a fluorinated surface by the reaction with F_2 molecules with energies greater than about 3.8 kcal/mol. However, diffraction measurements made after exposure of a clean Si(100) surface to higher energy F_2 show that Si−Si bonds on an unfluorinated surface are also disrupted by the reaction with higher energy F_2. The circles in Figure 5 represent the intensities of the specular, half-order and first-order diffraction features as a function of exposure to F_2 incident with 13 kcal/mol of energy and at a 6° angle. Unlike the measurements shown as solid lines in this figure, the He diffraction spectra were measured after a given F_2 exposure. Otherwise, the conditions of the He diffraction measurement are the same as discussed above.

The intensities of the diffraction features drop monotonically as the clean Si surface is initially exposed to F_2 incident at 13 kcal/mol. This initial decrease is expected, because the original periodicity of the clean (2 × 1)Si surface has been disrupted which results in the loss of coherency of the scattered He beam. However, in contrast to the recovery of the diffraction intensity as the coverage approaches 1 ML after exposure to low energy F_2, the diffracted intensity never recovers, indicating that the surface remains disordered. Even after exposure to sufficient high-energy F_2 to attain 1 ML coverage, the periodicity of the lattice does not recover.

Figure 9 shows the total SiF_2 and SiF_4 thermal desorption yields, $N_{SiF_2}(\Theta)$ and $N_{SiF_4}(\Theta)$, in arbitrary units, as a function of F_2 exposure for four F_2 translational energies. The F_2 beam is normal to the surface. Again, the SiF_2 yield is not sensitive to the incident F_2 energy, because it reflects the desorption kinetics of the final monolayer of fluorine. Rather, the increase in the fluorine saturation coverage is clear from the increase in the SiF_4 thermal desorption yield at high exposures. At high F_2 exposures of 20 ML F atoms, SiF_4 thermal desorption yield resulting from exposure to F_2 at 13 kcal/mol is roughly 2.5 times as large as that resulting from F_2 exposure at energies below 3.8 kcal/mol. Therefore, the saturation coverage increases by about 4.8%, to about 1.05 ML, as a result of exposure to F_2 at 13 kcal/mol. Similar effects of the incident F_2 energy on saturation coverage have been observed, but this previous work gives no information regarding the magnitude of the increase in the saturation coverage.[20] The observation that the saturation coverage increases beyond 1 ML coupled with the loss of surface order demonstrates that the translationally activated reaction occurs at Si−Si bonds even in the presence of dangling bonds.

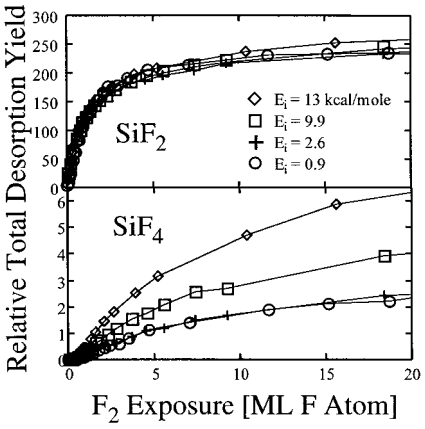

Figure 9. Total SiF_2 and SiF_4 thermal desorption yields, $N_{SiF_2}(\Theta)$ and $N_{SiF_4}(\Theta)$, measured at four total energies, E_i, as a function of F_2 exposure to a Si(100) surface with $\theta_i = 0°$. Solid lines connect the data points.

V. Discussion

A. Implications of Results. These studies have shown that the dissociative chemisorption probability of F_2 on a Si(100) surface covered with an ordered (2 × 1) overlayer of fluorine at 1 ML of coverage can be increased by raising the translational energy of the incident F_2 above 3.8 kcal/mol. The probability is observed to increase linearly with the normal component of the incident kinetic energy up to a value of about 3.6×10^{-3} at 13 kcal/mol, the highest energy experimentally attainable in this laboratory. Because these measurements are made on a Si surface saturated with fluorine, the threshold value for the translational energy is related to the barrier for dissociative chemisorption or reaction of F_2 with the Si−Si bonds as opposed to the Si dangling bonds. The similarity between the relative cross sections for diffusive scattering measured after exposure to translationally fast F_2 and those measured after Ar^+ ion bombardment strongly suggests that the reaction does not preferentially occur at the Si−Si dimer bonds.

Thus, these results confirm the presence of a significant barrier between the reactant and product states that arises from the repulsive interaction between the filled valence Si orbitals and the closed-shell F_2 molecule. This repulsive interaction can be overcome by increasing the translational energy of F_2 so that it can approach a Si lattice atom closely enough for a Si−F bonding interaction to form, and thus for Si−Si and F−F bond cleavage to occur. Cleavage of the Si−Si dimer bond apparently does not take place preferentially, even though it is likely a weaker bond than the bond between the first and second layer Si atoms. Calculations suggest that the bonds between the first layer Si atom and the three Si atoms below it are each weaker by an average of about 3 kcal/mol when a fluorine atom is

bonded to the first layer Si atom.[23] Since the dimer bond on the fluorinated surface is between two Si atoms each bonded to a fluorine atom, it is expected to be even weaker than the bonds of these two Si atoms to second layer Si atoms. Unfortunately, the calculated value that is available for the strength of the dimer bond between two Si atoms each bonded to a fluorine atom is 71 kcal/mol,[24] about 17 kcal/mol higher than the accepted value for a Si−Si bond in crystalline Si, 54 kcal/mol.[5] No explanation is provided for this deviation in the calculated value from expectation.[24] Regardless of the relative strengths of the Si−Si dimer and lattice bonds, it is likely that steric hindrance between the incoming F_2 molecule and the fluorine atoms bonded to each Si atom comprising the dimer is present, thus shielding the Si−Si dimer bonds from participation in the reaction, even if they are the weaker bonds.

The present experimental study emphasizes again[2] the observation that the exothermicity of the reaction of thermal energy F_2 with Si is not a source of lattice disorder. It is clear from the He diffraction spectrum that the Si(100)2 × 1 surface that has been saturated with fluorine incident with less than 3.8 kcal/mol maintains its well ordered (2 × 1) periodicity. This observation is in contrast to experimental and theoretical works that have suggested that the Si lattice disorders due to the large amount of energy released in the F_2 adsorption process.[25,26] However, when the collision energy of the F_2 incident on either the clean or fluorine-saturated Si surface is greater than 3.8 kcal/mol, disorder results because the incident F_2 has sufficient energy to overcome the barrier to reaction with the Si−Si bonds, thus disrupting the periodicity of the lattice. Therefore, it is clear that it is not the exothermicity but rather the collision energy that is ultimately effective in destroying the periodicity of an initially ordered lattice by its activation of the reaction.

Careful inspection of Figure 5 reveals that the intensity of the diffracted beams has mostly recovered by the time the F_2 exposure reaches 2 ML F atom. In contrast, Figure 3 shows that the saturation coverage of fluorine, 1 ML, is reached after a F_2 exposure of about 4 ML F atom. This seeming contradiction is reconciled by the small transfer width of the apparatus. Using the definition given by Comsa,[27] the transfer width of the apparatus is estimated as 35 Å, which is the largest periodicity that can be resolved. That is, ordered regions of the surface whose lengths are greater than 35 Å will not contribute to the intensity of the diffracted beams. Therefore, the coverage continues to increase as the size of the ordered regions grows with exposure while the intensity of the diffracted beams remains constant. The small transfer width is the result of the large entrance slits to the detector, which are purposely enlarged to optimize the signal for reactive scattering experiments.

Finally, the small effect of translational energy of the incident F_2 on its reaction with the Si−Si bonds is revealing. The dissociative chemisorption probability increases at most a factor of 4 as the translational energy is increased from 3.8 to 13 kcal/mol. In contrast, increases in the translational energy of a molecule incident on a metal surface over this same range are observed to increase the dissociative chemisorption probability by 2 to 3 orders of magnitude.[28−31] The inefficacy of translational energy in overcoming the barrier to dissociative chemisorption implies a potential energy surface with a late barrier, a barrier in the exit channel rather than the entrance channel.[32] In potential energy surfaces of this shape, vibrational excitation of the bond to be broken is more effective because vibrational motion aids in turning the corner into the exit channel where the barrier is positioned. Potential surfaces with late barriers may turn out to be characteristic of reactions on a Si lattice.

B. Comparison to Previous Results. *1. Effect of Translational Energy on Dissociative Chemisorption.* Unfortunately, a comparison of this result to other experimental studies of the effect of translational energy of a diatomic halogen molecule on its probability of dissociative chemisorption on a halogen-saturated Si surface is not possible. Previous studies have measured these effects either on a clean Si surface where the dissociative chemisorption probability is already close to 1[33−35] or on a Si surface whose coverage is changing from zero to a saturation value.[11,20,36] In both cases, the measurements reflect not only the effect of translational energy on dissociative chemisorption involving cleavage of Si−Si bonds but also on dissociative chemisorption involving the dangling bonds and the atom abstraction mechanism, which itself involves two channels, single-atom abstraction, and two-atom adsorption.

A comparison of these results to simulations can be made. A molecular dynamics simulation has recently been carried out to investigate the effect of the F_2 translational energy on the probability of its dissociative chemisorption on an ordered overlayer of 1 ML of fluorine on Si(100).[37] These calculations yield a barrier of approximately 58 kcal/mol for the dissociative chemisorption of F_2 on a fluorine-saturated surface. The value for this barrier is defined by the incident energy that yields an increase in the dissociation probability from zero to about 1×10^{-2}. This barrier is about 15 times larger than that observed experimentally, 3.8 kcal/mol, which is defined by the energy at which the dissociation probability increases beyond 9×10^{-4}. It is possible that an insufficient number of trajectories were employed in the simulation to achieve statistically significant values for the low dissociation probabilities at the lower translational energies. Unfortunately, the highest translational energy attainable for F_2 using seeded beam techniques is about 13 kcal/mol, so the dissociation probability at 58 kcal/mol cannot be measured experimentally and, hence, compared directly to the results of the simulation. However, linear extrapolation of the data in Figure 6 to 58 kcal/mol yields a dissociation probability of about 1.7×10^{-2}, a value that is not inconsistent with the calculated result. It should be recognized that this consistency is based on the assumption, for which there is no a priori reason, that the dissociation probability continues to increase linearly with the normal component of the incident energy above 13 kcal/mol. In addition, it is not clear whether the barrier in the simulation is derived from the total or normal translational energies.

The simulation also reveals that the barrier of 58 kcal/mol is associated with cleavage of the Si−Si lattice bonds. Reaction of F_2 with the Si−Si dimer bonds is not observed in the simulation until the F_2 incident energy is increased to about 115 kcal/mol. The higher barrier for reaction with the dimer bonds is concluded[37] to arise from the large repulsion between the adsorbed fluorine and the incoming F_2 molecule. The results from these simulations are consistent with our experimental result that the reaction of F_2 on a fluorine-saturated surface does not preferentially occur at the Si−Si dimer bonds, even though the Si−Si dimer bonds are weaker than the lattice bonds.

2. Effect of Translational Energy on Etching. There have been several previous experiments that have investigated the effect of the incident energy of Cl_2 on the rate of Si etching, where the etching rate is measured by the amount of volatile silicon chloride.[38−41] In general, these studies have found that increases in the energy of the incident Cl_2 result in an enhancement of the etching rate. However, in many of these studies,[38−40] no clear distinction is made between translational and internal state excitation of the incident Cl_2, so there is no consensus as to

their relative effects. But the germane point here is that a comparison of incident energy effects on the etching rate with those on the probability of dissociative chemisorption that are measured here is not necessarily straightforward. The probability of dissociative chemisorption measures the probability that an incident halogen molecule dissociates and that the resulting atoms bind to the surface. In contrast, the etching rate reflects the probabilities of all the processes that occur from the initial dissociative chemisorption to the reaction with the substrate and, finally, to the desorption of the product. Therefore, the effect of the incident energy on the etching rate could reflect not only its effect on the initial dissociative chemisorption probability but also on the reaction probability of the atoms deposited by the dissociative chemisorption of a prior molecule[42,43] or on the desorption probability of the product molecule.[44,45] In general, it is difficult to deconvolute the etching rate into the effect of incident energy on the individual steps of an etching reaction. However, in one case, the interaction of a hyperthermal beam of Cl_2 with Si, collision-induced desorption[44,45] of the $SiCl_4$ product has been noted, and the enhancing effect of translational energy on this step and, hence, of the etching rate has been studied.[41,46]

Acknowledgment. M.R.T., K.B.L., and M.T.S. gratefully acknowledge partial support through a NDSEG-ONR Predoctoral Fellowship, a NSF Postdoctoral Research Fellowship and, a NSF Predoctoral Fellowship, respectively. This work is supported by NSF CHE-9713276.

References and Notes

(1) Li, Y. L.; Pullman, D. P.; Yang, J. J.; Tsekouras, A. A.; Gosalvez, D. B.; Laughlin, K. B.; Zhang, Z.; Schulberg, M. T.; Gladstone, D. J.; Ceyer, S. T. *Phys. Rev. Lett.* **1995**, *74*, 2603. Ceyer, S. T. *Proc. R. A. Welch Found. Conf. Chem. Res. XXXVIII: Chemical Dynamics of Transient Species*; Welch Foundation: Houston, 1994; p 156−172. Pullman D. P.; Ceyer, S. T. *Abstracts of the ACS*; American Chemical Society: Washington, DC, *1994*; Vol. 207, p 168.

(2) Tate, M. R.; Gosalvez-Blanco, D.; Pullman, D. P.; Tsekouras, A. A.; Li, Y. L.; Yang, J. J.; Laughlin, K. B.; Eckman, S. C.; Bertino M. F.; Ceyer, S. T. *J. Chem. Phys.* **1999**, *111*, 3679.

(3) Tate, M. R.; Pullman, D. P.; Gosalvez-Blanco, D.; Tsekouras, A. A.; Li, Y. L.; Ceyer, S. T. *J. Chem. Phys.* **2000**, *112*, 5190.

(4) Wu, C. J.; Carter, E. A. *J. Am. Chem. Soc.* **1991**, *113*, 9061.

(5) Walsh, R. *Acc. Chem. Res*. **1981**, *14*, 246.

(6) Ceyer, S. T.; Gladstone, D. J.; McGonigal, M.; Schulberg, M. T. In *Physical Methods of Chemistry*, 2nd ed.; Rossiter, B. W., Baetzold, R. C., Eds.; Wiley: New York, 1993; Vol. IXA, p 383.

(7) Ishizaka, A.; Shiraki, Y. *J. Electrochem. Soc.* **1986**, *133*, 666.

(8) Winters, H. F.; Houle, F. A. *J. Appl. Phys.* **1983**, *54*, 1218.

(9) Engstrom, J. R.; Nelson, M. M.; Engel, T. *Phys. Rev. B* **1988**, *37*, 6563.

(10) Engstrom, J. R.; Nelson, M. M.; Engel, T. *Surf. Sci.* **1989**, *215*, 437.

(11) Behringer, E. R.; Flaum, H. C.; Sullivan, D J.; Masson, D. P.; Lanzendorf, E. J.; Kummel, A. C. *J. Phys. Chem.* **1995**, *99*, 12863.

(12) Yang, J. J. Ph.D. Thesis, Massachusetts Institute of Technology, Cambridge, MA, 1993.

(13) Gosalvez-Blanco, D. Ph.D. Thesis, Massachusetts Institute of Technology, Cambridge, MA, 1997.

(14) Shul, R. J.; Hayes, T. R.; Wetzel, R. C.; Baiocchi, F. A.; Freund, R. S. *J. Chem. Phys.* **1988**, *89*, 4042.

(15) Vasile, M. J.; Stevie, F. A. *J. Appl. Phys.* **1982**, *54*, 3799.

(16) Schulberg, M. T. Ph.D. Thesis, Massachusetts Institute of Technology, Cambridge, MA, 1990.

(17) Tate, M. R. Ph.D. Thesis, Massachusetts Institute of Technology, Cambridge, MA, 1999.

(18) Boland, J. J. *Adv. Phys.* **1993**, *42*, 129.

(19) Cardillo, M. J.; Becker, G. E. *Phys. Rev. B* **1980**, *21*, 1497.

(20) Behringer, E. R.; Flaum, H. C.; Kummel, A. C. *J. Phys. Chem.* **1995**, *99*, 5532.

(21) Poelsema, B.; Comsa, G. *Scattering of Thermal Energy Atoms from Disordered Surfaces*; Springer-Verlag: Berlin, 1989.

(22) Huang, L. J.; Lau, W. M.; Tang, H. T.; Lennard, W. N.; Mitchell, I. V.; Schultz, P. J.; Kasrai, M. *Phys. Rev. B* **1994**, *50*, 453.

(23) van den Hoek, P. J.; Ravenek, W.; Baerends, E. J. *Phys. Rev. B* **1988**, *38*, 12508.

(24) Wu, C. J.; Carter, E. A. *Phys. Rev. B* **1992**, *45*, 9065.

(25) Weakliem, P. C.; Wu, C. J.; Carter, E. A. *Phys. Rev. Lett.* **1992**, *69*, 200. Weakliem, P. C.; Carter, E. A. *J. Chem. Phys.* **1993**, *98*, 737. Carter, L. E.; Khodabandeh, S.; Weakliem, P. C.; Carter, E. A. *J. Chem. Phys.* **1994**, *100*, 2277.

(26) Lo, C. W.; Varekamp, P. R.; Shuh, D. K.; Durbin, T. D.; Chakarian, V.; Yarmoff, J. A. *Surf. Sci.* **1993**, *292*, 171.

(27) Comsa, G. *Surf. Sci.* **1979**, *81*, 57.

(28) Rettner, C. T.; Pfnur, H. E.; Auerbach, D. J. *Phys. Rev. Lett.* **1985**, *54*, 2716.

(29) Rettner, C. T.; DeLouise, L. A.; Auerbach, D. J. *J. Chem. Phys.* **1986**, *85*, 1131.

(30) Lee, M. B.; Yang, Q. Y.; Ceyer, S. T. *J. Chem. Phys.* **1987**, *87*, 2724.

(31) Rettner, C. T.; Stein, H. *Phys. Rev. Lett.* **1987**, *59*, 2768.

(32) Polanyi, J. C.; Wong, W. H. *J. Chem. Phys.* **1969**, *51*, 1439. Evans, M. G.; Polanyi, M. C. *Trans. Faraday. Soc*. **1939**, *35*, 178.

(33) Yan, C.; Jensen, J. A.; Kummel, A. C. *J. Chem. Phys.* **1995**, *102*, 3381.

(34) Doshita, H.; Ohtani, K.; Namiki, A. *J. Vac. Sci. Technol., A* **1998**, *16*, 265.

(35) Jensen, J. A.; Yan, C.; Kummel, A. C. *Science* **1995**, *267*, 493.

(36) Liu, Y.; Mason, D. P.; Kummel, A. C. *Science* **1997**, *276*, 1681.

(37) Carter, L. E.; Carter, E. A. *J. Phys. Chem.* **1996**, *100*, 873.

(38) Suzuki, K.; Hiraoka, S.; Nishimatsu, S. *J. Appl. Phys.* **1988**, *64*, 3697.

(39) Campos, F.; Weaver, G. C.; Waltman, C. J.; Leone, S. R. *J. Vac. Sci. Technol., B* **1992**, *10*, 2217.

(40) Teraoka, Y.; Nishiyama, I. *Appl. Phys. Lett*. **1993**, *63*, 3355.

(41) Szabo, A.; Engel, T. *J. Vac. Sci. Technol., A* **1994**, *12*, 648.

(42) Ceyer, S. T. *Science* **1990**, *249*, 133.

(43) Beckerle, J. D.; Johnson, A. D.; Yang, Q. Y.; Ceyer, S. T. *J. Chem. Phys.* **1989**, *91*, 5756.

(44) Beckerle, J. D.; Johnson, A. D.; Ceyer, S. T. *Phys. Rev. Lett.* **1989**, *62*, 685.

(45) Beckerle, J. D.; Johnson, A. D.; Ceyer, S. T. *J. Chem. Phys.* **1990**, *93*, 4047.

(46) Szabo, A.; Farrell, P. D.; Engel, T. *J. Appl. Phys.* **1994**, *75*, 3623.